ADVANCED FUNCTIONAL MATERIALS
www.afm-journal.de

Electrically Conductive Liquid Metal Composite Adhesives for Reversible Bonding of Soft Electronics

*A. B. M. Tahidul Haque, Dong Hae Ho, Dohgyu Hwang, Ravi Tutika, Chanhong Lee, and Michael D. Bartlett**

Conductive adhesives are required for the integration of dissimilar material components to create soft electronic and robotic systems. Here, a heterogeneous liquid metal-based conductive adhesive is developed that reversibly attaches to diverse surfaces with high stretchability (>100% strain), low modulus (<100 kPa), and strain-invariant electrical conductivity. This SofT integrated composite with tacK through liquid metal (STICK-LM) adhesive consists of a heterogeneous graded film with a liquid metal-rich side that is embossed at prescribed locations for electrical conductivity and an electrically insulating adhesive side for integration. Adhesion behavior is tuned for adhesion energies > 70 Jm^{-2} (≈ 25x enhancement over unmodified composites) and described with a viscoelastic analysis, providing design guidelines for controllable yet reversible adhesion in electrically conductive systems. The architecture of STICK-LM adhesives provides anisotropic and heterogeneous electrical conductivity and enables direct integration into soft functional systems. This is demonstrated with deformable fuses for robotic joints, repositionable electronics that rapidly attach on curvilinear surfaces, and stretchable adhesive conductors with nearly constant electrical resistance. This study provides a methodology for electrically conductive, reversible adhesives for electrical and mechanical integration of multicomponent systems in emerging technologies.

1. Introduction

The growing demand for ubiquitous soft electronic devices has prompted innovative technologies such as electronic skins, biomedical sensors, smart actuators, and soft robotics.[1–4] Developing these wearable and soft electronics necessitates material stretchability, flexibility, and compliance to conform to complex and dynamic substrates.[5,6] These applications also require the integration of dissimilar materials and components, which often entails adhesion for the joining of rigid and soft materials using methods such as elastomeric adhesion,[7–11] hydrogen bonding,[12–15] and chemical anchoring or covalent bonding.[16–18] This is required for the assembly of soft devices, the attachment and removal of these devices onto different surfaces or substrates, and the incorporation of multiple functional materials or components into 2D and 3D layouts. Although soft materials such as elastomers typically show some intrinsic adhesion, most unmodified elastomers do not show sufficient adhesion for reliable bonding to diverse surfaces.[19] Additionally, pristine elastomers or adhesives lack the necessary electrical conductivity for the transduction of electrical signals or power. Thus, electrically conductive materials with controllable adhesion for reversible bonding are key needs for these soft, emergent technologies.

To create soft materials with the required functionality to interface with integrated electronic components, intrinsically conductive polymers[20–22] are used or solid conductive fillers such as silver flakes,[23,24] silver nanowires,[25–27] and carbon nanotubes[28,29] are dispersed into or deposited onto elastomers. However, conductive polymers can have limited stretchability and high loadings of solid fillers in composites can increase the elastic modulus.[30–33] These characteristics can make adhesion more challenging, where stretchability and flexibility are needed to bond to complex surfaces and high modulus often increases the risk for detachment or delamination in extensible systems.[34–37]

Recently, liquid metal (LM)-based soft elastomeric composites have been studied as a method to overcome the mechanical compliance trade-off observed in solid filler conductive composites.[6,38–44] LM composites exhibit rich electrical properties and flexibility, even at high LM content, due to LM's high conductivity and fluidity.[45] Additionally, LM droplets can be assembled through techniques such as sedimentation, which

A. B. M. T. Haque, D. H. Ho, D. Hwang, R. Tutika, C. Lee, M. D. Bartlett
Mechanical Engineering
Soft Materials and Structures Lab
Virginia Tech
Blacksburg VA 24061, USA
E-mail: mbartlett@vt.edu

D. Hwang, R. Tutika, M. D. Bartlett
Macromolecules Innovation Institute
Virginia Tech
Blacksburg VA 24060, USA

The ORCID identification number(s) for the author(s) of this article can be found under https://doi.org/10.1002/adfm.202304101

DOI: 10.1002/adfm.202304101

accumulates droplets on one surface and direct ink write (DIW) processes to control the shape and orientation of droplets.[46,47] However, similar to other flexible electronics, LM composites face the problems of poor conformal contact and delamination from substrates. As a result, additional adhesive layers, encapsulation, or mechanical clamping are typically added to mount LM composites.[48,49] Alternative approaches for conformal adhesion have been developed, such as conductive interconnects,[50,51] adhesive inks that are fabricated directly on the substrate,[52] and tough, permanent LM composite adhesives.[18] To enable reversibility, recent research has focused on electroadhesion[53,54] and wet-adhesion[55,56] mechanisms, but they require external stimuli such as electricity, temperature, and/or humidity to activate and maintain adhesion. While progress has been made toward LM composite adhesives, achieving intrinsically reversible adhesion with patternable electrical conductivity offers new opportunities for the assembly of soft devices and their attachment and release onto diverse surfaces or substrates.

Here, we introduce a heterogeneous LM-based conductive adhesive that reversibly attaches to diverse surfaces with high stretchability (> 100%) and compliance (modulus < 100 kPa) while exhibiting strain-invariant electrical conductivity (**Figure 1**a,b). This SofT Integrated Composite with tacK through Liquid Metal (STICK-LM) consists of a heterogeneous graded film that is produced by sedimentation of LM droplets, leading to a LM-rich surface that can be embossed for electrical conductivity at prescribed locations, and an electrically insulating adhesive side (Figure 1c). The embossed traces leverage the liquid nature of the LM-conducive networks and show strain invariant resistance up to > 100% strain. The elastomer matrices are fabricated with an additional amine-based polymer to increase adhesion. The resulting composite exhibits adhesive energy > 70 Jm^{-2}, ≈ 25x higher than homogeneous silicone-based LM composites while also being electrically conductive. Additionally, the composite is reversible and reattachable to various surfaces as the debonding is primarily adhesive and not cohesive, contrasting approaches relying on strong or permanent adhesive layers. These qualities distinguish STICK-LM from other conductive adhesives. Some previous adhesives have shown high conductivity but low flexibility,[57,58] while others show good stretchability and adhesion but lack conductivity.[17,59] Furthermore, many of these adhesives are not reversible[17,58] or carry bulk conductivity,[60–62] making them susceptible to short-circuiting or requiring them to be patterned to isolate circuit components. The sedimentation assembly of LM droplets enables heterogeneous and anisotropic electric conductivity and allows for direct integration into functional systems without possible shorting through the thickness or dielectric side of the adhesive. We demonstrate this capability with an untethered, reattachable LED device that conforms to various curvilinear surfaces, a reversible attachable resistive heater for morphing materials, and a reusable adhesive fuse that passively and reversibly prevents overshoot in robotic joints.

2. Results and Discussion

2.1. Fabrication and Microstructure of Conductive-Adhesive Composites

The STICK-LM adhesive consists of LM (eutectic gallium indium (EGaIn)) droplets embedded in a silicone elastomer matrix. The elastomer is polydimethylsiloxane (PDMS) (Sylgard 184) to which we added a bulk distribution of a chemical additive ethoxylated polyethylenimine (PEIE). PDMS consists of siloxane precursors, which are catalyzed by a platinum curing agent. However, the amine-based polymer PEIE reacts with the curing agent and leaves unreacted precursor distributed throughout the matrix (Figure 1c second panel inset schematic). The PEIE plays three primary roles 1) It makes the composite more extensible and decreases the modulus. 2) It enhances the viscoelastic property of the elastomer matrix, which allows for the control of adhesion to different substrates. 3) The curing time of the elastomer matrix increases, which facilitates the sedimentation of denser LM droplets and develops the heterogeneous microstructure. These characteristics facilitate the creation of a heterogeneous LM structure and enable the control of the electrical and adhesive properties of the composite.

The LM droplet size directly affects the sedimentation kinetics and the resulting heterogeneous microstructure. In order to settle, the weight of the LM droplets has to overcome the buoyancy and drag forces in the liquid phase elastomer.[46,63] Therefore, we tuned the shear mixing conditions to control the LM droplet size.[64] We studied shear mixing speeds of 600 and 1200 rpm to determine the effect of droplet sizes on LM sedimentation. The micrographs and droplet distribution analysis of Figure S1 (Supporting Information) demonstrate different droplet diameters of 58 ± 29 μm and 35 ± 17 μm for composites mixed at 600 and 1200 rpm, respectively. Figure S2 (Supporting Information) shows that larger droplets settle and have a high LM concentration on one side whereas smaller droplets are found distributed throughout the thickness. Energy-dispersive X-ray spectroscopy (EDS) in Figure 1d further shows the settling behavior of larger droplets with a distinct LM (i.e., gallium (Ga) and indium (In)) rich side and PDMS-PEIE (i.e., silicon (Si)) rich side. This heterogeneous microstructure was quantitatively evaluated through a thresholded, binary image analysis in Figure 1e where LM and matrix are respectively marked by dark and bright regions. The cross section is divided into six 500 μm thick striations and the number of dark pixels is calculated to find the LM fraction in each segment. The relative composition of LM and silicone as a function of depth is plotted in Figure 1f, which shows a gradual increase of LM from < 20% at top to ≈70% in the bottom section. Clearly, the large LM droplets from the 600 rpm mixing ensure pre-curing settlement and enable a heterogeneous microstructure. This creates an insulating adhesion surface and an LM rich surface. As the settled LM droplets are critical for electrical percolation by embossing, the large LM droplets are used for the remainder of the study.

2.2. Adhesion and Mechanical Properties

The PEIE curing modifier and functional LM inclusions alter the mechanical and adhesion properties of the composites. This is attributed to a reduction of elastic modulus, which improves contact formation with a substrate as well as a tuning of the viscoelastic behavior of the composites to increase adhesion energy. This combination allows for strong, reversible adhesion through physical van der Waals interactions and dissipation through fingering instabilities characteristic of soft adhesive materials (**Figure 2**a). To understand the effect of PEIE and LM inclusions on adhesion,

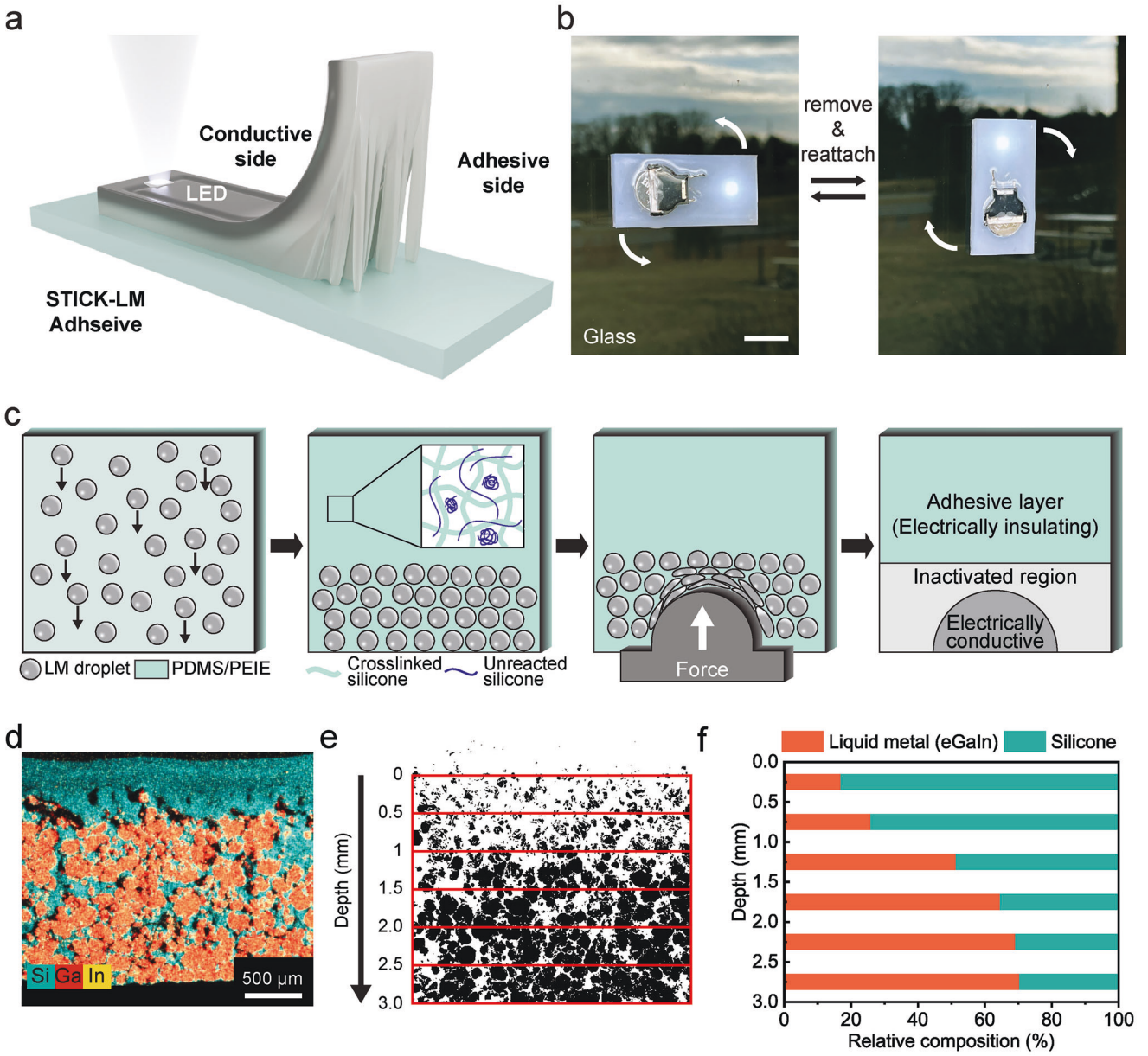

Figure 1. Heterogeneous, liquid metal-based STICK-LM conductive adhesives. a) Schematic of the heterogeneous SofT Integrated Composite with tacK through Liquid Metal (STICK-LM) adhesive as a reattachable LED device. b) Photograph of relocating the reattachable LED device on top of an outdoor glass surface. Scale bar is 2 cm. c) Schematic of the fabrication process for the heterogeneous and adhesive LM composite microstructure in a PDMS-PEIE elastomer matrix. d) Cross-sectional SEM/EDS image of the settled liquid metal droplets inside the elastomer matrix e) Binary image of the SEM/EDS image where the red outlines show the 500 μm thick striations for through thickness compositional image analysis. f) Volume percentage of LM inside the composite as a function of film depth.

we performed 90° peel testing (Figure 2b). Without the PEIE curing modifier, the silicone elastomer and LM composites debond without fingering instabilities and show low peel forces. However, upon the addition of a small concentration of 0.4 vol% PEIE, the peel forces substantially increased for both PDMS-PEIE and STICK-LM (PDMS-PEIE-LM) composites. The adhesives fail adhesively and show fingering instabilities at the interface as shown in Figure 2a. A PEIE concentration of 0.4 vol% is the maximum for adhesive failure and will be used for the rest of the study. At a PEIE concentration of 0.5 vol%, peel forces were lower than at 0.4 vol% and cohesive failure was observed during debonding with debris left behind on the surface (Figure S3, Supporting Information).

The adhesion performance can be characterized by adhesion energy (G_c), which indicates the debonding resistance of an adhesive (Figure 2c). The value is calculated by averaging the data points in the plateau peel force regime in Figure 2b. While PDMS and PDMS-LM show an adhesion energy of 4.9 and 2.9 Jm^{-2}, PDMS-PEIE and STICK-LM show enhanced adhesion energy up to 66.5 and 72.2 Jm^{-2}, respectively. Specifically, the addition of

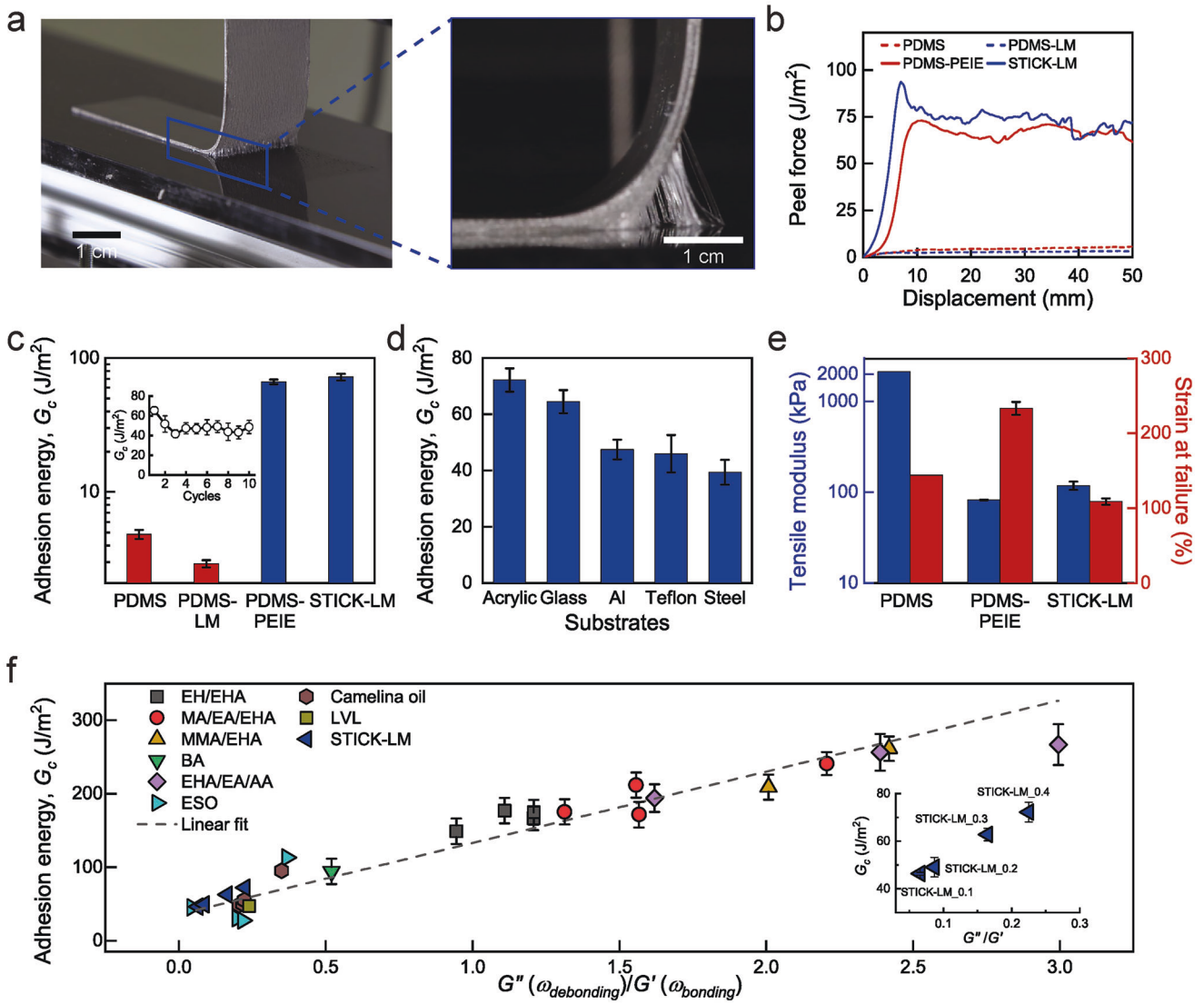

Figure 2. Adhesive composite properties and design. a) Photograph of a STICK-LM peel test and side view. b) 90° peel data to measure adhesion energy for PDMS, PDMS-LM, PDMS-PEIE, and STICK-LM on an acrylic plate. c) Comparison of adhesion energy (G_c) values for the specimens. d) STICK-LM adhesion energy on different substrates. Error bars represent the standard deviation of the peel plateau region in a single cycle in c and d. e) Tensile modulus and strain at failure of PDMS, PDMS-PEIE, and STICK-LM composites. Error bars represent the standard deviation for n = 3. f) Correlation between peel energy and $G''(\omega_{debonding})/G'(\omega_{bonding})$. Polymers are based on ethyl acrylate (EA), 2-ethylhexyl acrylate (EHA), methyl acrylate (MA), methyl methacrylate (MMA), butyl acrylate (BA), acrylic acid (AA),[65] epoxidized soybean oil/lactic acid oligomers (ESO),[66] camelina oil derivatives (Camelina oil),[67] poly(lactide-b-β-methyl-δ-valerolactone-b-lactide) triblock copolymer) (LVL).[68] Inset graph shows results of STICK-LM at different PEIE volume concentrations. Error bars of the experimental data represent the standard deviation for n = 5. Literature data error bars are gathered from the references.

PEIE into the PDMS-LM matrix enables a ≈ 25x increase in G_c in STICK-LM over the PEIE-free PDMS-LM. The composite also continues to function over multiple cycles of bonding and releasing (Figure 2c; Figure S4, Supporting Information) and is applicable to diverse substrates including acrylic, glass, aluminum, Teflon, and steel (Figure 2d; Figure S4b, Supporting Information). The strong, reversible adhesion of the STICK-LM on diverse substrates over the PEIE-free counterpart is attributed to the ability to flow and wet the surface over a short contact time, often known as tack, while dissipating energy during debonding.

Mechanical properties that contribute to adhesion, such as stiffness and extensibility are also influenced by PEIE and LM droplets as seen in Figure 2e (stress–strain data are presented in Figure S5, Supporting Information). Through the addition of PEIE, the tensile modulus of PDMS decreases from nearly 2,000 kPa to below 100 kPa, and the strain at failure increases from 150% to nearly 230%. By adding LM droplets into the PEIE-PDMS matrix, the modulus of STICK-LM becomes ≈100 kPa with a stain at break over 100%. This decrease in modulus of the STICK-LM adhesive over the PEIE-free LM composite enables tacky adhesion characteristics. This can be explained by the Dahlquist criterion, where adhesive tack appears when the modulus is approximately 100 kPa or less.[69] Importantly, the modulus remains relatively unaffected and meets the Dahlquist criterion

even with LM, highlighting the fluid nature of the LM droplets that helps maintain high compliance in these soft composites. The relative modulus insensitivity of the PDMS-PEIE matrix due to LM inclusions can enable synergistic opportunities to achieve reversible adhesion and controlled electrical properties arising from the dispersed LM droplets.

To describe the adhesive characteristics of these soft composites we consider that the adhesion energy during peel is correlated to rheological material parameters G'' and G',[65] such that:

$$G_c \approx G''(\omega_{debonding})/G'(\omega_{bonding}) \quad (1)$$

G'' is the loss modulus and is associated with dissipation, which is important during the debonding process when dissipative processes can control the peel energy. G' is the storage modulus and is associated with contact formation, which is relevant during the bond formation process. Each rheological parameter adopts a different frequency due to the two distinct time scales of debonding (a more rapid process) and the bond formation process (a relatively slower process). The model shows that in order to increase the adhesion energy, the loss modulus at the debonding frequency needs to be increased to enhance the dissipative effect while lowering the storage modulus at the bonding frequency to conform to a substrate. In Figure 2f, we plot adhesion energy (G_c) as a function of $G''(\omega_{debonding})/G'(\omega_{bonding})$ and find good agreement with our STICK-LM adhesives as well as a variety of pressure sensitive adhesives (PSAs) (literature data from Refs. [65–68]). This plot provides a clear design criteria for soft, viscoelastic adhesive materials. For example, for the reversible conductive adhesives in this study relatively lower $G''(\omega_{debonding})/G'(\omega_{bonding})$ ratios are desired, to enable bond strength while still allowing for reversibility. By contrast, to enable stronger more permanent adhesives, the $G''(\omega_{debonding})/G'(\omega_{bonding})$ ratio should be increased. This is commonly achieved in the design of PSAs through polymer parameters such as molecular weight or through additives such as tackifying hydrocarbon resins and plasticizers.[70] In our STICK-LM adhesives, PEIE enhances $G''(\omega_{debonding})/G'(\omega_{bonding})$ and thus G_c, while not increasing dissipation to such an extent as to degrade the reversibility of the adhesives. These results demonstrate that repositionable and reversible conductive adhesives can be created through the addition of PEIE into liquid metal-based silicone elastomers by controlling viscoelasticity, providing guidance for conductive adhesive design.

2.3. Electrical and Electro-Mechanical Properties

An electrically conductive STICK-LM adhesive can be created through stretching, which can activate the entire LM rich side of a sample, or through embossing on the LM rich side, which can create selective conductive regions.[71] The stretching-induced electrical activation of the STICK-LM adhesives is examined for film thicknesses of 0.5, 1.0, and 1.5 mm (**Figure 3**a), which shows that only the 1.5 mm thickness sample becomes conductive. The resistance of the STICK-LM adhesive drops to nearly 10 Ωcm^{-1} (sample length is 3 cm), indicating activation of the entire LM-rich layer. The embossing activation for STICK-LM adhesives with the three thicknesses is also examined, which shows that 1.0 and 1.5 mm thickness specimens are activated reaching low resistances of 3 and 1 Ωcm^{-1}, respectively, while the 0.5 mm sample never activates (Figure S8, Supporting Information). Irrespective of the activation method, the adhesive side remains insulated due to the controlled segregation of LM droplets through settling during initial fabrication. This enables anisotropic electrical conductivity, where the adhesive is conductive in plane but not through thickness. Therefore, we can fabricate different types of STICK-LM adhesives based on activation methods and thickness control. These include a non-conductive composite, an electrically anisotropic and heterogeneous conductive composite, which shows in-plane selective electrical paths on a single side through embossing, and another anisotropic composite, which shows in-plane conductivity across a single side of the composite through stretching.

The electro-mechanical behavior of a 1 mm thick STICK-LM adhesive, which provides the ability to emboss a circuit pattern and avoids short-circuiting by external strain, is presented in Figure 3b. Here, the instantaneous resistance R is normalized by the initial resistance R_0 during cyclic loading (25% strain increments up to 100%). Three consecutive full loading cycles are applied to the specimen and the ratio R/R_0 remains stable after a 25% decrease in the first cycle. The decrease in resistance is attributed to the further rupture of LM droplets in the embossed electric region to form a more connected network (the non-embossed region stays electrically insulating as seen in Figure S9, Supporting Information). The electrical conductivity also remains stable during strain and hold experiments, showing a minimal effect of viscoelasticity on the electrical conductivity (Figure S10, Supporting Information).

The electrical properties are also examined while bonded to stretchable (rubber sheet) or flexible substrates (PET film). Figures 3c,d show the electrical resistance (R/R_0) of the STICK-LM adhesive remains nearly constant during 100% stretching or 50% compression bending strain. This combination of conductive yet adhesive characteristics is shown by stretching a "VT" shaped STICK-LM adhesive bonded to a stretchable rubber film. The adhesive side of the composite is used to attach to the rubber film while the conductive side has embossed circuit traces to power LEDs (Figure 3e). When the rubber film is stretched, the STICK-LM adhesive deforms with the substrate and the LEDs remain functional.

2.4. Demonstration of STICK-LM Adhesive as a Soft, Reattachable Heater

The adhesion characteristics and electrical conductivity of the STICK-LM adhesive make it a promising candidate for soft reattachable heaters. By applying an electrical bias to the embossed electrodes, Joule heating can be realized (**Figure 4**a) and the average temperature can be measured on the heater surface (red dotted area) with a maximum temperature of 100 °C at 5 V bias. The applied current and the power input of the soft reattachable heater are plotted in Figure 4b. As the current is increased, the current-voltage relation shows a linear correlation, which indicates that the electrical resistance of the embossed circuit does not change due to heat generation. At 5 V, the soft heater consumes 4.5 W of electric energy, with a watt density of 0.33 Wcm^{-2}.

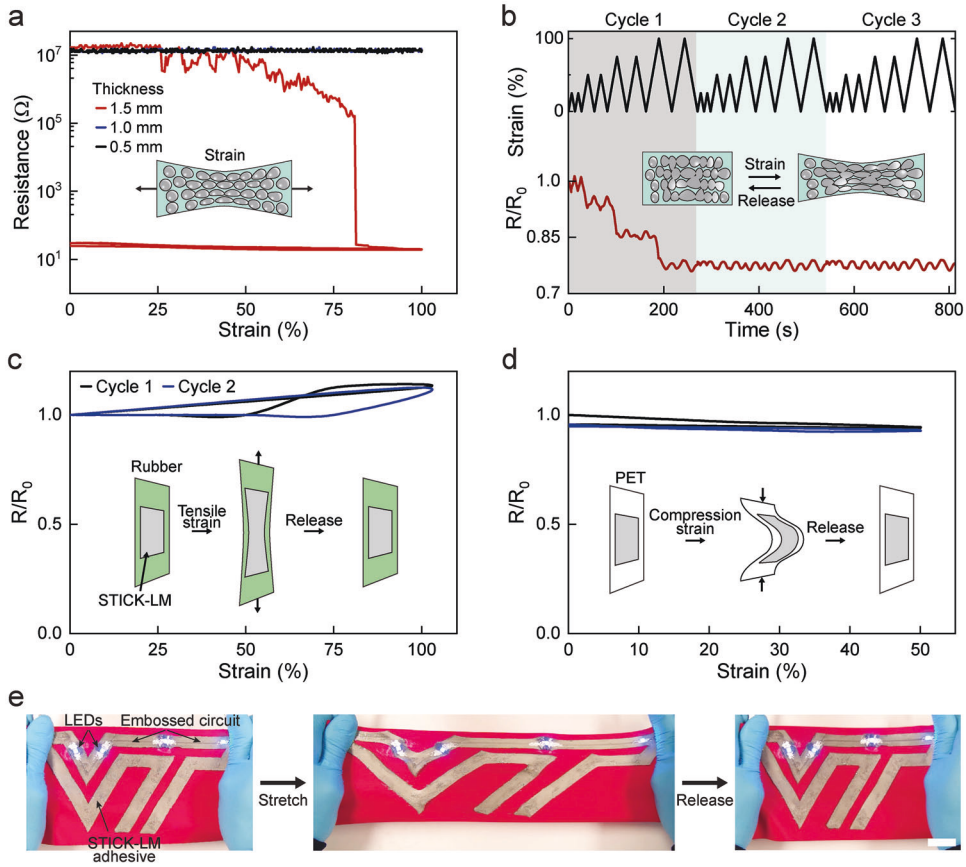

Figure 3. Electro-mechanical behavior of LM adhesive composite. a) Stretching induced activation of STICK-LM adhesive with different film thicknesses. b) Cyclic loading and resistance response of a 1 mm thick STICK-LM adhesive for three incremental stretching cycles. Color shaded areas show periods of cycles 1, 2, and 3. c) Resistance response of a STICK-LM adhesive bonded to a rubber substrate and stretched to 100% tension strain where the inset schematic shows the measuring procedure. d) Resistance response of a STICK-LM adhesive bonded to a PET film and bent to 50% compression strain where the inset schematic shows the measuring procedure. e) Stretching a 'VT' shaped STICK-LM adhesive bonded to a stretchable rubber film, which is stretched and then released. Scale bar is 25 mm.

The temporal-thermal behavior of the STICK-LM adhesive heater depends on the applied voltage, which is measured over a range of 0.5–5 V and is plotted in Figure 4c. Consecutive heating and cooling cycles of 300 s were performed and the average temperature was recorded. The results indicate that the temperature increases for 300 s which is in good agreement with power consumed by the STICK-LM in Figure 4b.

To demonstrate the use of STICK-LM adhesive as a soft, reattachable heater, an architectured Field's metal embedded morphing kirigami sheet is utilized as shown in the Figure 4d schematic. Field's metal is a low melting point alloy which has a melting point at 62°C. Below the melting point, the alloy is in a solid state and the kirigami structure maintains its shape as shown in the right image of Figure 4d. To locally morph the structure, the soft STICK-LM adhesive heater is sequentially attached to and removed from each leg of the morphing structure (first and second images in Figure 4e). When a voltage bias of 4.5 V is applied to the embossed circuit on the heater, the temperature reaches 85 °C, which melts the Field's metal and causes the morphing material to change shape from a concave to convex configuration (Figure 4e; Video S1, Supporting Information). The adhesion characteristics enable STICK-LM adhesive to attach to and create a conformal contact with the morphing material for efficient heat transfer. This example of the STICK-LM adhesive heater demonstrates the reusable adhesive characteristics in conjunction with the electrical conductivity and heat transfer properties to enable morphing. Such adhesive, reusable soft heaters can be employed in a range of thermally activated actuating or morphing systems that require the rapid transfer of heat at different locations while maintaining conformal contact.

2.5. Soft Electronics Demonstration of Reattachable STICK-LM Adhesives

STICK-LM adhesives can function as soft circuit boards for electronics that are reattachable on-demand to diverse surfaces. We demonstrate this by using a reattachable LED device, which is fabricated with on-board power and a LED connected through an embossed STICK-LM circuit (**Figure 5**a). To evaluate the device in real-world environments, it is attached to various untreated surfaces such as a car body, grey dolomite/limestone, a paper box (Figure 5b), and an aluminum panel (Figure S11 and Video S2, Supporting Information). The LED device shows stable

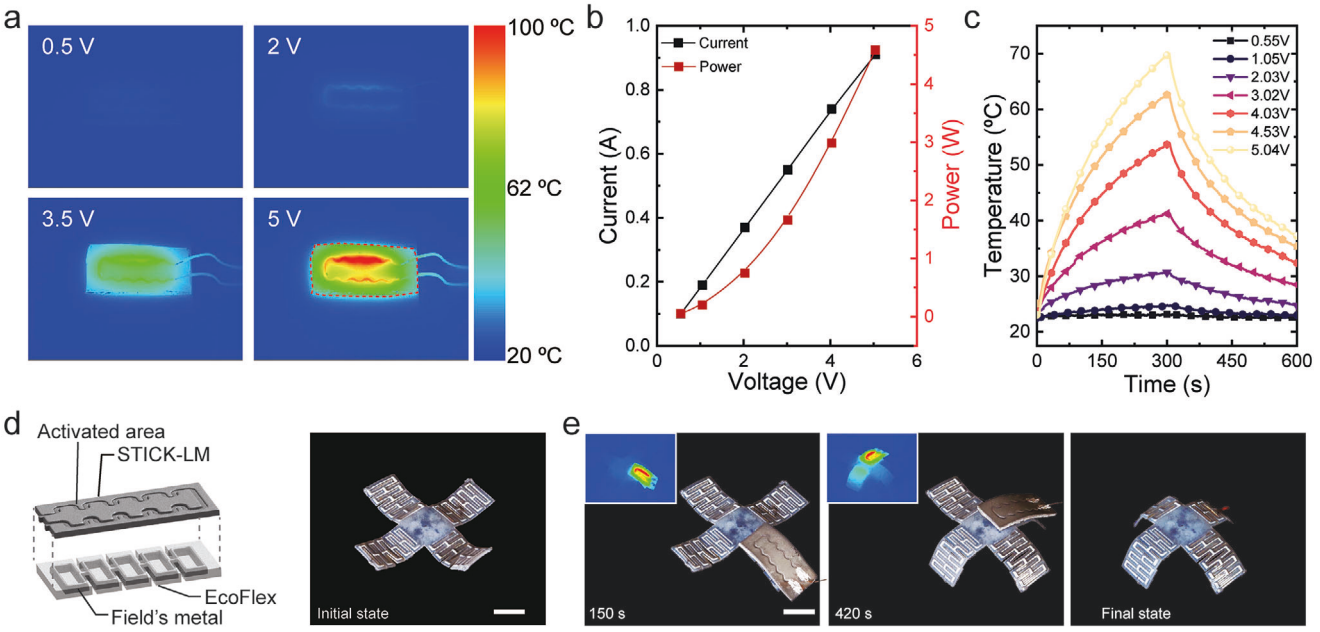

Figure 4. Demonstration of STICK-LM adhesive as a reattachable soft heater for morphing materials. a) A series of IR images with voltage bias. b) Current and power as a function of voltage applied to the STICK-LM adhesive. c) The heating and cooling properties of the STICK-LM adhesive as a function of applied voltage bias. d) Schematic of the morphing material sheet and the STICK-LM adhesive attached to the top of the material. Image on the right shows the initial state of the morphing material sheet. e) A series of images showing the shape change in the morphing material sheet due to the heat applied through a STICK-LM adhesive heater. Inset IR image color palette scale is same as the color bar in component a). White scale bars are 20 mm.

adhesion behavior independent of the surface roughness. Additionally, the adhesive surface of the reattachable LED device can instantly bond to the selected surface. In Figure 5c, three powered on LED devices are tossed onto a vertical car window, which illustrates rapid bonding and robust electrical and mechanical stability (Video S3, Supporting Information). After an aging period of six months, the reattachable LED device is tested and found to maintain its adhesion and electrical characteristics on various substrates (Figure S12a, Supporting Information). Additionally, a cyclic adhesion and detachment test is performed with the aged device over 100 times on a car window surface (Figure S12b and Video S4, Supporting Information). Throughout the test, the device maintained both its electrical conductivity and adhesion characteristics.

We further demonstrate STICK-LM adhesive as a soft resettable fuse for a robotic arm that uses electro-mechanical protection in contrast to traditional fuses that are based on charge carrier effects. The movement of a robotic arm needs to have a range of limited motion to avoid impact with surrounding objects or to prevent self-damage. Conventional control systems have utilized software limits to impose restrictions on the robotic arm movement based on motor feedback signals. However, an electrical system malfunction, such as an overshooting signal can override the software control. To protect damage from an overshot signal, we adopted STICK-LM adhesives that serve as both an electrode for relaying signals as well as a stretchable and resettable mechanical fuse. As shown in the schematic of Figure 5d, when the robotic joint functions in the specified motion range, the STICK-LM adhesive works as an electrode to relay signals. When the signal overshoots due to environmental disturbance or control system malfunction, the bending angle exceeds the set angle threshold, leading to the detachment of the STICK-LM adhesive from the surface of the robotic arm. As a result, the electrical connection between the power supply and the motor is lost and thereby avoiding a potential damage event. As the STICK-LM adhesive functions as a resettable multi-use fuse, it can be reattached to the robotic arm. Figure 5e shows the fabricated robotic arm with the STICK-LM adhesive as a stretchable mechanical fuse at a rotation joint.

As demonstrated in Figure 5f and Video S5 (Supporting Information), from 0 to 35 s, the robotic joint operates in the specified motion range. At 35 s, the simulated overshooting signal was applied to the motor, causing excessive actuation. As a result, the STICK-LM adhesive fuse detached from one side of the joint and protected it from permanent damage. This detached fuse can be reattached to the joint and can again function as a fuse as shown in Figure 5f image (t = 70 s). At 90 s, a second simulated overshooting signal was applied to the robotic joint and the fuse again detached from the joint. This STICK-LM fuse prevents damage over multiple cycles and can be reattached to restart the robotic motion.

3. Conclusion

STICK-LM adhesives simultaneously achieve reversible adhesion, high compliance, stetchability, and electrical conductivity which can be tuned through thickness and patterned across plane. Through LM sedimentation and embossing, STICK-LM adhesives display anisotropic and heterogeneous electrical conductivity. This provides a new design space and overcomes

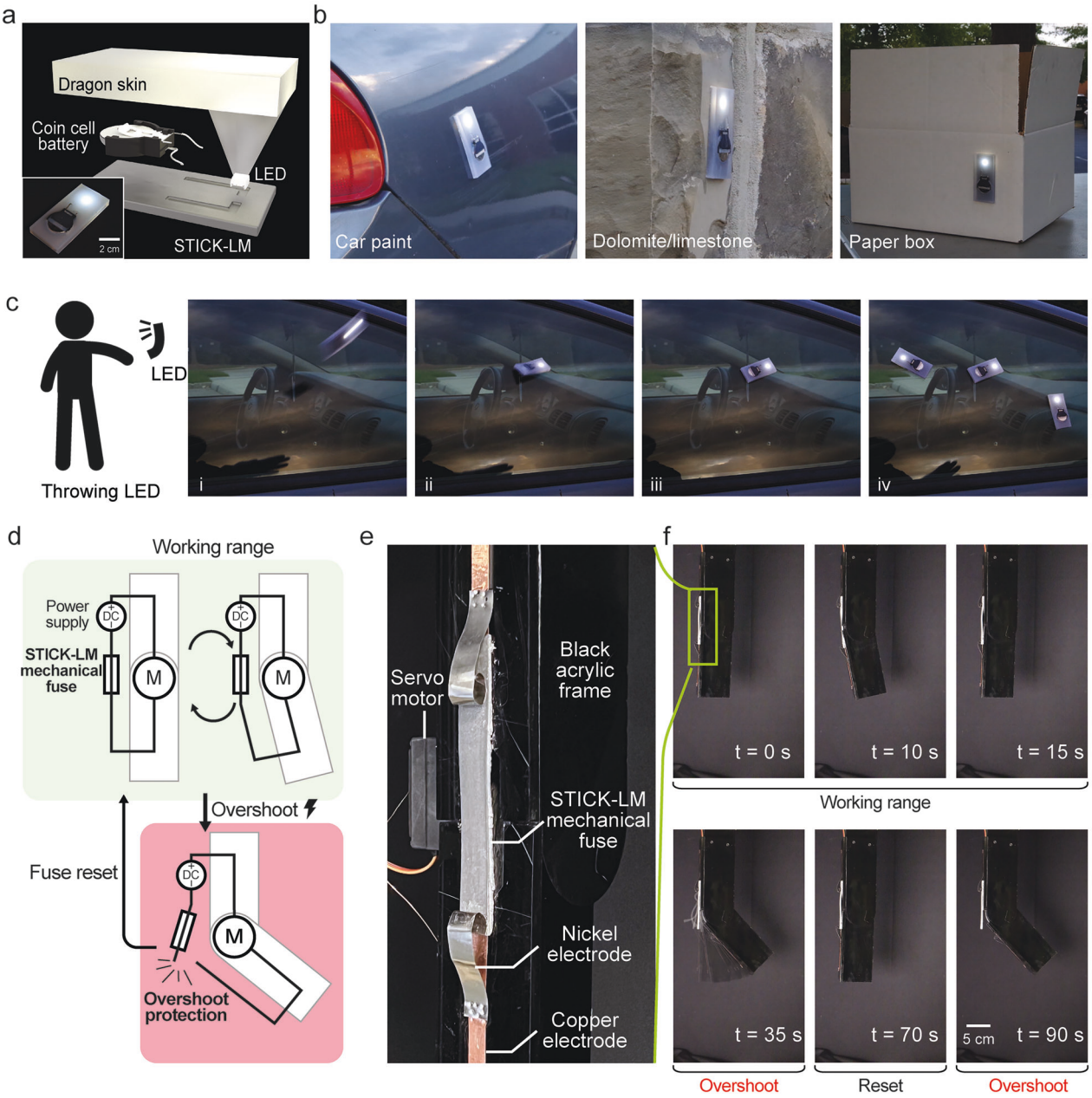

Figure 5. Demonstration of STICK-LM adhesive as a reattachable LED and mechanical fuse. a) Schematic of the structure of the reattachable LED and inset photograph shows the assembled device. b) Photographs of the reattachable LED adhered to the various substrates. c) Photographs show reattachable LEDs thrown on and sticking to a car window. d) Schematic diagram of the STICK-LM mechanical fuse in use and its overshoot regulation behavior. e) Photograph of the assembled robotic joint with a STICK-LM mechanical fuse. f) Series of photographs show the regular behavior of the robotic joint from 0 to 15 s, at 35 s simulated overshooting occurred and a STICK-LM mechanical fuse regulated the irregular movement. At 70 s, the STICK-LM fuse was reset and another simulated overshooting occurred at 90 s, and the STICK-LM mechanical fuse again regulated the irregular movement.

challenges in conductive adhesives where electrical conductivity is commonly isotropic and homogeneous, which can hinder the integration of multicomponent systems. Through the control of droplet morphology and rheological behavior, reversible adhesives are enabled. Particularly, we provide design rules by tuning the viscoelastic properties, which can aid in the future development of electrically conductive adhesives. Combined with the non-specific bonding, STICK-LM adhesives can rapidly bond to a variety of surfaces, be removed, and then be reattached over multiple cycles. The liquid nature of the LM droplets allows for the maintenance of soft mechanical response and provides strain-invariant electrical resistance. These properties make STICK-LM adhesive useful for a variety of soft electronic, soft robotics, and morphing material applications and provide a strategy for multifunctional, adhesive bonding and integration.

4. Experimental Section

Composite Film Fabrication: Composites were fabricated by mixing a two-component Pt-cure poly(dimethyl siloxane) (PDMS) elastomer at a 10:1 silicone precursor to curing agent weight ratio (Sylgard 184; Dow) with polyethylenimine (PEIE) (80% ethoxylated solution; Sigma–Aldrich). Liquid phase PDMS was shear mixed with a controlled volume of PEIE (held constant at 0.4 vol% except in Figure 2f where it was varied from 0 to 0.5 vol%) in a dual asymmetric centrifugal (DAC) mixer (Flaktek Speedmixer). The liquid metal (LM) used in this study was Eutectic Gallium Indium (EGaIn; Rotometals Inc.) which was an alloy of gallium and indium at 3:1 weight ratio. The individual metals were added to a glass jar and heated at 200°C for 24 h on a hot-plate to obtain the eutectic phase of LM. The LM was dispersed at 50 vol% loading in the liquid phase matrix (PDMS and PEIE) by shear mixing in the DAC mixer. To cast the composite, a 0.5 mm thin elastomer bed (PDMS 10:1) was prepared on a glass slide and Ease release 200 (Smooth-On Inc.) was sprayed on the surface. The composite was cured at room temperature for 6 h to allow the settling of LM droplets. Then the composite was completely cured in a convection oven at 80°C for 24 h.

SEM Analysis: SEM images of sample cross-sections were obtained on a FEI Quanta 600 FEG-SEM in back-scattered electron (BSE) mode at a spot size of four and an accelerating voltage of 20 kV. The samples were immersed in liquid nitrogen to freeze the liquid metal droplets prior to cutting with a razor blade to prepare thin cross-sections for SEM analysis. EDS was performed using Bruker QUANTAX 400 detector to evaluate the elemental composition of the sample cross-sections.

Morphology Analysis: Droplet size and distribution were analyzed from SEM and optical micrographs using Fiji software. The images were converted to binary, droplet areas were calculated and the droplet dimensions were extracted from the best fit ellipse to the area. For distributions, the major diameter of the ellipses was plotted as histograms to obtain the mean and standard deviations from Gaussian fits.

Mechanical Characterization: *Tension test*: The tensile modulus and failure strain of materials were obtained according to ASTM D412. The dogbone shaped specimens were cut from composite sheet using a 50% standard die. An Instron 5944 mechanical testing machine equipped with a 500 N load cell was used to deform the samples at the rate of 1 mm s^{-1}. For each set of tests, three composites were tested and the tensile modulus was calculated from the stress–strain curve up to a strain of 5% using a linear fit algorithm in MATLAB.

Frequency Dependent Mechanical Properties: To obtain the material's mechanical behavior at bonding and debonding frequencies, the samples were tested on a TA instruments Q850 DMA. Rectangular specimens with length 10 mm and width 5 mm were tested over a frequency range of ω = 0.06–628 $rads^{-1}$ and presented in Figures S6 and S7 (Supporting Information). At the peel rate of 1 mm s^{-1} and an adhesive thickness of 1.5 mm, the debonding and bonding frequencies were calculated to be 4.2 and 0.06 $rads^{-1}$, respectively. The storage modulus at 0.06 $rads^{-1}$ and loss modulus values at 4.2 $rads^{-1}$ were used to calculate the ratio of loss modulus to storage modulus (E''/E'). The ratio of shear loss modulus to storage modulus (G''/G') was calculated through the $G = E/2(1 + \nu)$, where ν is Poisson's ratio.

Adhesion measurement: The adhesion energy (G_c) between an adhesive strip and an acrylic substrate was measured using a 90°peel test setup on an Instron 5944 mechanical tester at a displacement rate of 1 mm s^{-1}. G_c was calculated over a range of 30 mm displacement iin the plateau region.

Embossing Activation: Embossing was used to activate electrical traces on the LM settled side of the composite. A plastic mold with a 1 mm thick and 3 mm long embossing feature (B9 Core five Series XL - 405, B9Creations, LLC) was used to apply compressive load by an Instron 5944 mechanical testing machine to indents up to 70% of the film thickness. Copper tapes were attached to two edges of the mold to monitor the activation of composite. Composite conductivity was measured through a Keithley 2460 Source Measuring Unit (SMU), which was connected to conductive copper tapes attached at two edges of the embossing mold. Constant current was supplied and voltage change was measured during compression at 10 mm s^{-1}. The electrical and mechanical measurement instruments were synced to correlate the mechanical embossing parameters (force, displacement) and resistance of composites. MATLAB was used to synchronously start the recording and trigger off the instruments when a threshold of deformation or resistance was reached.

Strain-Resistance Characterization: The strain-resistance measurement during the cyclic and step-hold tests of the conductive–adhesive composites was performed using rectangle specimen of dimension 3 cm × 1 cm. Before the strain tests, we activated 3 cm long conductive line on each composite using the embossing technique. Copper tape was used to connect the conductive line of a composite to a Keithley 2460 SMU. The copper tapes were clamped inside grippers to ensure that the measured resistance corresponds only to the stretched films. Mechanical stretching was performed on an Instron 5944 mechanical testing machine and resistance was measured using Keithley 2460 SMU. The final resistance and strain data were synchronized in a post-processing step using MATLAB.

Statistical Analysis: The meaning of all error bars was described within the captions of the corresponding figures. Statistical analysis was done using the computer program Origin Pro.

Supporting Information

Supporting Information is available from the Wiley Online Library or from the author.

Acknowledgements

A.B.M.T.H., D.H.H., and D.H. contributed equally to this work. The authors acknowledge support from NSF (No. CMMI-2238754), Defense Advanced Research Projects Agency Young Faculty Award (DARPA YFA) (D18AP00041), and the Institute for Critical Technology and Applied Science (ICTAS) at Virginia Tech. This work was performed in part at the Nanoscale Characterization and Fabrication Laboratory, which was supported by the Virginia Tech National Center for Earth and Environmental Nanotechnology Infrastructure (NanoEarth), a member of the National Nanotechnology Coordinated Infrastructure (NNCI), supported by NSF (ECCS 1542100 and ECCS 2025151).

Conflict of Interest

The authors declare no conflict of interest.

Data Availability Statement

The data that support the findings of this study are available from the corresponding author upon reasonable request.

Keywords

adhesive, composites, elastomers, liquid metals, soft electronics

Received: April 13, 2023
Revised: June 13, 2023
Published online:

[1] R. F. Shepherd, F. Ilievski, W. Choi, S. A. Morin, A. A. Stokes, A. D. Mazzeo, X. Chen, M. Wang, G. M. Whitesides, *Proc. Natl. Acad. Sci.* **2011**, *108*, 20400.
[2] J. Ramírez, D. Rodriquez, A. D. Urbina, A. M. Cardenas, D. J. Lipomi, *ACS Appl. Nano Mater.* **2019**, *2*, 2222.

[3] Z. Peng, Y. Shi, N. Chen, Y. Li, Q. Pei, *Adv. Funct. Mater.* **2021**, *31*, 1.
[4] A. Mohammadi Nasab, S. Sharifi, S. Chen, Y. Jiao, W. Shan, *Adv. Intell. Syst.* **2021**, *3*, 2000166.
[5] C. J. Thrasher, Z. J. Farrell, N. J. Morris, C. L. Willey, C. E. Tabor, *Adv. Mater.* **2019**, *31*, 1.
[6] Y. Han, L. E. Simonsen, M. H. Malakooti, *Adv. Energy Mater.* **2022**, *12*, 2201413.
[7] A. M. Nasab, A. Luo, S. Sharifi, K. T. Turner, W. Shan, *ACS Appl. Mater. Interfaces* **2020**, *12*, 27717.
[8] N. Deneke, A. L. Chau, C. S. Davis, *Soft Matter* **2021**, *17*, 863.
[9] S. H. Jeong, S. Zhang, K. Hjort, J. Hilborn, Z. G. Wu, *Adv. Mater.* **2016**, *28*, 5830.
[10] Y. Jiang, S. Ji, J. Sun, J. Huang, Y. Li, G. Zou, T. Salim, C. Wang, W. Li, H. Jin, J. Xu, S. Wang, T. Lei, X. Yan, W. Y. X. Peh, S. C. Yen, Z. Liu, M. Yu, H. Zhao, Z. Lu, G. Li, H. Gao, Z. Liu, Z. Bao, X. Chen, *Nature* **2023**, *614*, 456.
[11] G. Wan, Y. Tang, K. T. Turner, T. Zhang, W. Shan, *Adv. Funct. Mater.* **2023**, *33*, 2209905.
[12] R. Wang, T. Xie, *Langmuir* **2010**, *26*, 2999.
[13] B. Liu, Y. Wang, Y. Miao, X. Zhang, Z. Fan, G. Singh, X. Zhang, K. Xu, B. Li, Z. Hu, M. Xing, *Biomaterials* **2018**, *171*, 83.
[14] T. Zhang, A. R. Gans-Forrest, E. Lee, X. Zhang, C. Qu, Y. Pang, F. Sun, T. Luo, *ACS Appl. Mater. Interfaces* **2016**, *8*, 33326.
[15] H. G. Nam, M. G. Nam, P. J. Yoo, J. H. Kim, *Soft Matter* **2019**, *15*, 785.
[16] J. M. Taylor, K. Perez-Toralla, R. Aispuro, S. A. Morin, *Adv. Mater.* **2018**, *30*, 1705333.
[17] H. Yuk, T. Zhang, S. Lin, G. A. Parada, X. Zhao, *Nat. Mater.* **2016**, *15*, 190.
[18] T. A. Pozarycki, D. Hwang, E. J. Barron III, B. T. Wilcox, R. Tutika, M. D. Bartlett, *Small* **2022**, *18*, 2203700.
[19] M. D. Bartlett, S. W. Case, A. J. Kinloch, D. A. Dillard, *Prog. Mater. Sci.* **2023**, *137*, 101086.
[20] S. Peng, Y. Yu, S. Wu, C. H. Wang, *ACS Appl. Mater. Interfaces* **2021**, *13*, 43831.
[21] Y. Wang, C. Zhu, R. Pfattner, H. Yan, L. Jin, S. Chen, F. Molina-Lopez, F. Lissel, J. Liu, N. I. Rabiah, Z. Chen, J. W. Chung, C. Linder, M. F. Toney, B. Murmann, Z. Bao, *Sci. Adv.* **2017**, *3*, e1602076.
[22] H. Yuk, B. Lu, S. Lin, K. Qu, J. Xu, J. Luo, X. Zhao, *Nat. Commun.* **2020**, *11*, 1.
[23] C. Cano-Raya, Z. Z. Denchev, S. F. Cruz, J. C. Viana, *Appl. Mater. Today* **2019**, *15*, 416.
[24] L. Mo, Z. Guo, L. Yang, Q. Zhang, Y. Fang, Z. Xin, Z. Chen, K. Hu, L. Han, L. Li, *Int. J. Mol. Sci.* **2019**, *20*, 2124.
[25] J. Lee, P. Lee, H. Lee, D. Lee, S. S. Lee, S. H. Ko, *Nanoscale* **2012**, *4*, 6408.
[26] S. Yao, J. Yang, F. R. Poblete, X. Hu, Y. Zhu, *ACS Appl. Mater. Interfaces* **2019**, *11*, 31028.
[27] S. Kang, S. Cho, R. Shanker, H. Lee, J. Park, D. S. Um, Y. Lee, H. Ko, *Sci. Adv.* **2018**, *4*, eaas8772.
[28] A. Kamyshny, S. Magdassi, *Small* **2014**, *10*, 3515.
[29] S. Park, M. Vosguerichian, Z. Bao, *Nanoscale* **2013**, *5*, 1727.
[30] A. D. Printz, A. V. Zaretski, S. Savagatrup, A. S.-C. Chiang, D. J. Lipomi, *ACS Appl. Mater. Interfaces* **2015**, *7*, 23257.
[31] Y. Yang, H. Deng, Q. Fu, *Mater. Chem. Front.* **2020**, *4*, 3130.
[32] G. Hu, C. Zhao, S. Zhang, M. Yang, Z. Wang, *Polymer* **2006**, *47*, 480.
[33] F. Du, R. C. Scogna, W. Zhou, S. Brand, J. E. Fischer, K. I. Winey, *Macromolecules* **2004**, *37*, 9048.
[34] L. Xiao, M. Cheng, F. Chen, S. Jiang, Y. A. Huang, *J. Appl. Mech.* **2022**, *89*, 031005.
[35] G. Palasantzas, J. T. M. D. Hosson, *Phys. Rev. E* **2003**, *67*, 021604.
[36] G. Violano, L. Afferrante, A. Papangelo, M. Ciavarella, *J. Adhes.* **2019**, *97*, 509.
[37] L. Pastewka, M. O. Robbins, *Proc. Natl. Acad. Sci. USA* **2014**, *111*, 3298.
[38] M. D. Bartlett, A. Fassler, N. Kazem, E. J. Markvicka, P. Mandal, C. Majidi, *Adv. Mater.* **2016**, *28*, 3726.
[39] Y. Y. Choi, D. H. Ho, J. H. Cho, *ACS Appl. Mater. Interfaces* **2020**, *12*, 9824.
[40] S. G. Wallace, N. P. Bradshaw, N. X. Williams, J. H. Qian, K. W. Putz, C. E. Tabor, M. C. Hersam, *Adv. Mater. Technol.* **2022**, *7*, 2101178.
[41] A. B. M. T. Haque, R. Tutika, M. Gao, A. Martinez, J. Mills, J. Arul Clement, J. Gao, M. Tabrizi, M. Ravi Shankar, Q. Pei, M. D. Bartlett, *Multifunct. Mater.* **2020**, *3*, 4.
[42] A. Martin, C. Du, A. M. Pauls, T. Ward, M. Thuo, *Adv. Mater. Interfaces* **2020**, *7*, 2001294.
[43] G. G. Guymon, M. H. Malakooti, *J. Polym. Sci.* **2022**, *60*, 1300.
[44] K. Zheng, F. Gu, H. Wei, L. Zhang, X. Chen, H. Jin, S. Pan, Y. Chen, S. Wang, *Small Methods* **2023**, *7*, 2201534.
[45] M. D. Dickey, *Adv. Mater.* **2017**, *29*, 1606425.
[46] M. J. Ford, D. K. Patel, C. Pan, S. Bergbreiter, C. Majidi, *Adv. Mater.* **2020**, *32*, 46.
[47] A. Haake, R. Tutika, G. M. Schloer, M. D. Bartlett, E. J. Markvicka, *Adv. Mater.* **2022**, *34*, 2200182.
[48] M. D. Bartlett, N. Kazem, M. J. Powell-Palm, X. Huang, W. Sun, J. A. Malen, C. Majidi, *Proc. Natl. Acad. Sci.* **2017**, *114*, 2143.
[49] S. Liu, D. S. Shah, R. Kramer-Bottiglio, *Nat. Mater.* **2021**, *20*, 851.
[50] J. Dou, L. Tang, L. Mou, R. Zhang, X. Jiang, *Compos. Sci. Technol.* **2020**, *197*, 108237.
[51] L. Mou, J. Qi, L. Tang, R. Dong, Y. Xia, Y. Gao, X. Jiang, *Small* **2020**, *2005336*, 1.
[52] M. A. Rahim, F. Centurion, J. Han, R. Abbasi, M. Mayyas, J. Sun, M. J. Christoe, D. Esrafilzadeh, F. M. Allioux, M. B. Ghasemian, J. Yang, J. Tang, T. Daeneke, S. Mettu, J. Zhang, M. H. Uddin, R. Jalili, K. Kalantar-Zadeh, *Adv. Funct. Mater.* **2021**, *31*, 1.
[53] S. Park, J. Shintake, E. Piskarev, Y. Wei, I. Joshipura, E. Frey, T. Neumann, D. Floreano, M. D. Dickey, *Adv. Mater. Technol.* **2021**, *2100263*, 1.
[54] H. Lu, G. Yun, T. Cole, Y. Ouyang, H. Ren, J. Shu, Y. Zhang, S. Zhang, M. D. Dickey, W. Li, S.-Y. Tang, *ACS Appl. Mater. Interfaces* **2021**, *13*, 37904.
[55] J. Cheng, J. Shang, S. Yang, J. Dou, X. Shi, X. Jiang, *Adv. Funct. Mater.* **2022**, *32*, 2200444.
[56] D. Pei, S. Yu, P. Liu, Y. Wu, X. Zhang, Y. Chen, M. Li, C. Li, *Adv. Funct. Mater.* **2022**, *32*, 2204257.
[57] Y. Ko, J. Oh, K. T. Park, S. Kim, W. Huh, B. J. Sung, J. A. Lim, S. S. Lee, H. Kim, *ACS Appl. Mater. Interfaces* **2019**, *11*, 37043.
[58] Y. Xin, S. Zhang, Y. Lou, J. Xu, J. Zhang, *Adv. Mater. Technol.* **2020**, *5*, 2000018.
[59] Y. Wang, A. Gozen, L. Chen, W. H. Zhong, *Adv. Energy Mater.* **2017**, *7*, 6.
[60] J. Luo, Z. Cheng, C. Li, L. Wang, C. Yu, Y. Zhao, M. Chen, Q. Li, Y. Yao, *Compos. Sci. Technol.* **2016**, *129*, 191.
[61] J. Chen, J. Liu, T. Thundat, H. Zeng, *ACS Appl. Mater. Interfaces* **2019**, *11*, 18720.
[62] L. Zhang, K. S. Kumar, H. He, C. J. Cai, X. He, H. Gao, S. Yue, C. Li, R. C. S. Seet, H. Ren, J. Ouyang, *Nat. Commun.* **2020**, *11*, 1.
[63] C. Pan, D. Liu, M. J. Ford, C. Majidi, *Adv. Mater. Technol.* **2020**, *5*, 1.
[64] R. Tutika, S. Kmiec, A. B. M. T. Haque, S. W. Martin, M. D. Bartlett, *ACS Appl. Mater. Interfaces* **2019**, *11*, 17873.
[65] H. W. H. Yang, *J. Appl. Polym. Sci.* **1995**, *55*, 645.
[66] Y. Li, D. Wang, X. S. Sun, *RSC Adv.* **2015**, *5*, 27256.
[67] Y. Li, X. S. Sun, *Ind. Crops Prod.* **2015**, *73*, 73.
[68] T. R. Ewert, A. M. Mannion, M. L. Coughlin, C. W. Macosko, F. S. Bates, *J. Rheol.* **2018**, *62*, 161.
[69] K. Autumn, C. Majidi, R. Groff, A. Dittmore, R. Fearing, *J. Exp. Biol.* **2006**, *209*, 3558.
[70] S. Sun, M. Li, A. Liu, *Int. J. Adhes. Adhes.* **2013**, *41*, 98.
[71] R. Tutika, A. T. Haque, M. D. Bartlett, *Commun. Mater.* **2021**, *2*, 64.